IEEE Access
Multidisciplinary | Rapid Review | Open Access Journal

Received December 21, 2017, accepted February 15, 2018, date of publication March 7, 2018, date of current version March 19, 2018.

Digital Object Identifier 10.1109/ACCESS.2018.2810139

Range-Angle Localization of Targets With Planar Frequency Diverse Subaperturing MIMO Radar

XINGXING LI[1], DANGWEI WANG[1], WEN-QIN WANG[2], (Senior Member, IEEE), WEIJIAN LIU[3], (Member, IEEE), AND XIAOYAN MA[1]

[1]Air Force Early Warning Academy, Wuhan 430010, China
[2]School of Communication and Information Engineering, University of Electronic Science and Technology of China, Chengdu 610054, China
[3]Wuhan Electronic Institute, Wuhan 430205, China

Corresponding author: Xingxing Li (li_x_xing@163.com)

ABSTRACT Target localization utilizing frequency diverse array (FDA) has received much attention in recent years. In this paper, we propose a tensor subspace-based multiple-target 3-D localization method with planar frequency diverse subaperturing multiple-input multiple-output (FDS-MIMO) radar. To fully exploit the inherent multidimensional FDS-MIMO radar matched filter output information, a tensor signal model is established first. Then, the FDS-MIMO radar range ambiguity problem is mitigated by applying co-prime frequency offsets along both the dimensions of the planer array. Next, a beamspace-based unitary tensor-multiple signal classification (UTMUSIC) algorithm is developed to utilize the inherent multidimensional structure through the higher order singular value decomposition (HOSVD)-based low-rank approximation. Moreover, two computationally efficient methods, namely, partial spectral search UTMUSIC and range-angle decoupling UTMUSIC algorithms, are also proposed accordingly. The superiority of the proposed approaches over conventional methods is verified with numerical results, in terms of both computational complexity and estimation accuracy.

INDEX TERMS Frequency diverse array (FDA), transmit subaperturing, target localization, range ambiguity, co-prime frequency offset, tensor MUSIC.

I. INTRODUCTION

Target localization is one of the most important tasks required for a variety of applications including radar [1], sonar, wireless communications [2] and others fields. Phase-array radar (PAR) and multiple-input multiple-output (MIMO) radar have been widely employed for target localization. Nevertheless, their beam steering is fixed in an angle for all ranges. Consequently, the range and angle information of targets cannot be directly estimated from the beamforming output. However, in some applications such as range-ambiguous clutter and interferences suppression, it is a desired ability to control the energy distribution in a range-angle sector of interest.

In the last few years, a more flexible array radar named frequency diverse array (FDA) radar was proposed [3], [4], whose essence lies in that a small frequency increment across the array antennas is employed to produce range-angle-dependent beampattern. Recently, FDA radar has drawn a remarkable amount of attention in radar community owing to its particular beampattern [5]–[10]. By exploiting the FDA potential benefits, improved radar performance over traditional PAR and MIMO radar can be attained, such as beampattern synthesis [11]–[17], high-resolution imaging [18], [19], range-ambiguous clutter and interference suppression [20], [21], multipath mitigation [22], [23], and target localization [24]–[27].

The range-angle-dependent beampattern potentially afford a way to estimate the range and angle of a target simultaneously. Nevertheless, it is not accessible for a standard FDA radar due to the range-angle coupling in the beam domain. Several strategies have been developed to solve this problem, which can be generally classified into three types:

1) Linear array with nonuniform element inter-spacings. In [23], a nonuniform linear FDA is suggested for bistatic radar which is subsequently developed for range-angle imaging of targets [28], but it is not practical in real life because of the requirements of relocating the elements mechanically.

2) Linear array with nonuniform frequency increments. Non-linear frequency increments such as logarithmic [14], square, cubic [29], and sinusoid increasing frequency

offsets [30] are suggested. However, these methods will result in high sidelobes. The author of [31] proposed a focused beampattern by optimizing the frequency offsets with genetic algorithm. Nevertheless, the optimized frequency offsets are dependent on the desired range and angle sector. That is, the frequency offsets must be optimized again when the scanning region varies, which requires considerably high complexity.

3) Combined frequency offsets or co-array structure. A double-pulse uniform linear array (ULA) is investigated for targets localization [26], [32]. The subarray-based solutions divide the FDA antennas into multiple subarrays to handle the coupling problem [25], [33]. The essence of the above methods is that two frequency increments are used to decouple the range-angle beampattern. In [34], an interesting FDA scheme using co-prime frequency increments is proposed for linear FDA. Besides, nested-array is also employed for FDA to estimate range and angle of targets [35], [36].

Although the beampattern is decoupled in [25], [26], [32], and [33], the FDA radar still confronts range ambiguity problem due to its beampattern periodicity. In [24], a joint range and angle estimation method is presented to handle the range ambiguity, but *a priori* target range estimate is needed and a constraint on the frequency increments must be satisfied. Non-linear frequency offsets can alleviate the ambiguity, but the high sidelobes will degrade the beamforming performance [14], [29], [30].

In addition, the aforementioned approaches are primarily developed for a linear array FDA. In practice, 2D FDA is also an interesting topic. In [37], planar FDA geometries are initially discussed. Furthermore, the target localization performance of the planar MIMO-OFDM radar is investigated [38]. More noticeably, matrix-based processing is only considered in existing FDA target localization methods such as beamforming [26], [32], maximum likelihood estimator (MLE) [24] and MUSIC [25]. Obviously, this operation ignores the multidimensional information structure inherent in the received FDA signals. Consequently, the parameter estimation performance will degrade.

In this paper, we present an FDA and MIMO hybrid frequency diverse subaperturing MIMO (FDS-MIMO) radar structure. First, multilinear algebra [39] is introduced into FDS-MIMO radar to exploit the multidimensional structure information inherent in the received signals. Then, a unitary tensor MUSIC (UTMUSIC) method is developed for multiple-target localization. Furthermore, to alleviate tremendous spectral search, we propose two new dimension- reduced methods, namely, partial spectral search (PPS) UTMUSIC and range-angle decoupling (RAD) UTMUSIC.

The main contributions of this paper are summarized as follows:

1) A planar FDS-MIMO radar scheme with a co-prime frequency increment design strategy is proposed for multiple-target localization, which circumvents the range ambiguity problems in existing FDA methods.

2) A theoretical framework of HOSVD-based low-rank approximation subspace estimation approach is proposed for the FDS-MIMO radar. To our knowledge, this is the first time to use tensor subspace technique for FDA-related applications. This method exploits the inherent multidimensional structure of received data to improve target localization performance.

3) To reduce computation burden for the UTMUSIC algorithm, we also introduce two computational efficient implementations. Both methods achieve higher target localization accuracy at high signal-to-noise ratio (SNR) and significantly low complexity as compared to [38].

The remainder of this paper is organized as follows. Section II formulates the tensor signal model for FDS-MIMO radar. Section III analyzes the range ambiguity problem, and then presents an elimination strategy. Next, the UTMUSIC-based FDS-MIMO radar multiple-target localization algorithm is proposed, and two novel dimension-reduced algorithms are developed, along with their complexity analysis in Section IV. Finally, extensive numerical results and performance comparisons are provided in Section V, and conclusions are drawn in Section VI.

Notations: $(\cdot)^T$, $(\cdot)^*$, $(\cdot)^H$, and $(\cdot)^+$ represent the transpose, conjugate, conjugate transpose, and matrix Moore-Penrose pseudo-inverse, respectively. $\otimes$, $\odot$, $\circ$, and $\oplus$ symbolize the Kronecker product, Hadamard product, outer product, and Khatri-Rao product, respectively. The n-mode product of $\boldsymbol{\mathcal{A}} \in \mathbb{C}^{I_1 \times I_2 \times \cdots \times I_N}$ with a matrix $\mathbf{X} \in \mathbb{C}^{J_n \times I_n}$ is defined as $\boldsymbol{\mathcal{Y}} = \boldsymbol{\mathcal{A}} \times_n \mathbf{X} \in \mathbb{C}^{I_1 \times I_2 \times \cdots \times I_{n-1} \times J_n \times I_{n+1} \times \cdots \times I_N}$, where $y_{i_1,i_2,\ldots,i_{n-1},j_n,i_{n+1},\ldots,i_N} = \sum_{i_n=1}^{I_n} a_{i_1,i_2,\ldots,i_N} x_{j_n,i_n}$. $\|\cdot\|_2$, $\|\cdot\|_F$ and $\|\cdot\|_H$ represent vector 2-norm, matrix Frobenius norm, and higher-order tensor norm, respectively. $\mathbf{I}_p$ denotes a $p \times p$ identity matrix. $\mathbf{\Pi}_p$ represents the $p \times p$ exchange matrix with ones on its antidiagonal and zeros elsewhere. The unitary matrix $\mathbf{Q}_p \in \mathbb{C}^{p \times p}$ is the left-$\mathbf{\Pi}$-real matrices satisfying $\mathbf{\Pi}_p \mathbf{Q}_p^* = \mathbf{Q}_p$, which has the following form

$$\mathbf{Q}_{2p+1} = \frac{1}{\sqrt{2}} \begin{bmatrix} \mathbf{I}_p & 0 & j\mathbf{I}_p \\ \mathbf{0}_{1\times p} & \sqrt{2} & \mathbf{0}_{1\times p} \\ \mathbf{\Pi}_p & 0 & -j\mathbf{\Pi}_p \end{bmatrix} \tag{1}$$

where $\mathbf{Q}_{2p}$ can be obtained by dropping its central row and central column.

II. TENSOR SIGNAL MODEL OF FDS-MIMO RADAR

Fig. 1 illustrates a planar FDA radar geometry. The FDA elements are divided into multiple non-overlapping uniform rectangular subarrays. The transmitted waveforms among the subarrays are orthogonal and a small frequency increment across the subarray elements is employed, while the waveform transmitted in each subarray is coherent. The first element in the first subarray is taken as the origin point (point A) and the reference antenna. The radar consists of $M \times N$ elements and contains $P \times Q$ subarray, where M and N denote the number of elements along the x' and z'-axes, P and Q represent the number of subarrays along the

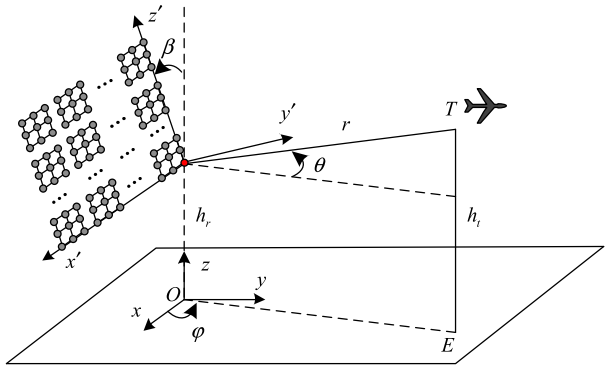

FIGURE 1. Basic Geometry of the FDS-MIMO radar.

x' and z'-axes, respectively. In doing so, each subarray contains $K_x = M/P$ elements along the x'-axes and $K_z = N/Q$ elements along the z'-axes, respectively. The adjacent element spacing at each axes are denoted by d_x and d_z, respectively. In some practical applications, the planar array is usually oblique, we suppose the inclination angle is β. In the radar coordinate system $Ax'y'z'$, the position vector of the (m, n)-antenna is

$$\mathbf{r}'_{mn} = (x_m, 0, z_n)^T, \quad m = 1, 2, \ldots, M, \ n = 1, 2, \ldots, N \tag{2}$$

where $x_m = (m-1)d_x$ and $z_n = (n-1)d_z$. In the target coordinate system $Oxyz$, h_r denotes the altitude from the reference point A to reflective surface. According to the space Cartesian coordinate relation, the position vector of the (m, n)-antenna in the coordinate system $Oxyz$ is given by

$$\mathbf{r}_{mn} = \mathbf{C}_r \mathbf{r}'_{mn} + (0, 0, h_r)^T \tag{3}$$

with $\mathbf{C}_r$ being

$$\mathbf{C}_r = \begin{bmatrix} 1 & 0 & 0 \\ 0 & \cos\beta & -\sin\beta \\ 0 & \sin\beta & \cos\beta \end{bmatrix}. \tag{4}$$

The line-of-sight (LOS) range difference between the (m, n)-antenna and point A is

$$d_{mn}(\theta, \varphi) = [\mathbf{r}_{mn} - (0, 0, h_r)]^T \mathbf{a}_r = \left(\mathbf{C}_r \mathbf{r}'_{mn}\right)^T \mathbf{a}_r \tag{5}$$

where the normalized LOS direction vector $\mathbf{a}_r = \mathbf{r}/r$ in the target coordinate system can be written as

$$\mathbf{a}_r = (\cos\theta\cos\varphi, \cos\theta\sin\varphi, \sin\theta)^T. \tag{6}$$

Then, the transmit steering vector associated with the (p, q) -subarray can be expressed as

$$\mathbf{a}_{pq}(\theta, \varphi) = \left[\mathbf{a}_p(\theta, \varphi) \circ \mathbf{a}_q(\theta, \varphi)\right] \odot A_{pq}(\theta, \varphi) \tag{7}$$

where

$$\mathbf{a}_p(\theta, \varphi) = \left[1, \ldots, \exp\left(j2\pi f_{pq}(K_x - 1)d_{21}(\theta, \varphi)/c\right)\right]^T \tag{8}$$

$$\mathbf{a}_q(\theta, \varphi) = \left[1, \ldots, \exp\left(j2\pi f_{pq}(K_z - 1)d_{12}(\theta, \varphi)/c\right)\right]^T \tag{9}$$

$$A_{pq}(\theta, \varphi) \approx \exp\left(j2\pi \frac{f_b}{c}\left[(p-1)K_x d_{21}(\theta, \varphi) + (q-1)K_y d_{12}(\theta, \varphi)\right]\right) \tag{10}$$

Here, $A_{pq}(\theta, \varphi)$ denotes the (p, q)-element of the transmit angular steering matrix $\mathbf{A}(\theta, \varphi)$. f_{pq} is the carrier frequency in the (p, q)-subarray given by

$$f_{pq} = f_c + (p-1)\Delta f_x + (q-1)\Delta f_z, \quad p = 1, 2 \ldots P, \quad q = 1, 2 \ldots Q \tag{11}$$

where Δf_x and Δf_z represent the frequency offsets along the x' and z'-axes, respectively. Considering the fact that $(p-1)\Delta f_x + (q-1)\Delta f_z \ll f_c$, the equivalent carrier frequency can be written as $f_b = f_c + (P-1)\Delta f_x/2 + (Q-1)\Delta f_z/2$. For convenience, we define the following vector

$$\mathbf{F}(\gamma, C) = \left[1, \exp(j\gamma), \cdots, \exp(j(C-1)\gamma)\right]^T. \tag{12}$$

Then, we have

$$\mathbf{A}(\theta, \varphi) = \mathbf{F}(2\pi f_b K_x d_{21}(\theta, \varphi)/c, P) \circ \mathbf{F}(2\pi f_b K_z d_{12}(\theta, \varphi)/c, Q). \tag{13}$$

The signal emitted from the (p, q)-subarray can be expressed as

$$s_{pq}(t) = \text{rect}\left(\frac{t}{T}\right)\phi_{pq}(t)\exp\left(j2\pi f_{pq}t\right) \tag{14}$$

where T is the pulse width. The signals $\phi_{pq}(t)$ are orthogonal with each other, i.e.,

$$\int_T \phi_{pq}(t)\phi^*_{uv}(t-\tau)\exp\left(j2\pi(p-u)\Delta f_x t\right) \cdot \exp\left(j2\pi(q-v)\Delta f_y\right)dt = 0, \quad p \neq u \ and \ q \neq v \tag{15}$$

where τ is an arbitrary time delay.

Under point target assumption, the transmitted signals incident on the target can be modeled as

$$s_t(t) = \sum_{p=1}^{P}\sum_{q=1}^{Q} \mathbf{w}_{pq}^H \mathbf{a}_{pq}(\theta, \varphi)A_{pq}(\theta, \varphi)s_{pq}(t - r/c) \tag{16}$$

where $\mathbf{w}_{pq}$ is the weight vector of the (p, q)-subarray, c is the speed of light. The reflected signals received by the receiving (m, n)-antenna in the lth pulse has the form

$$x_{m'n'l}(t) = \sum_{p=1}^{P}\sum_{q=1}^{Q} \beta_l \mathbf{w}_{pq}^H \mathbf{a}_{pq}(\theta, \varphi)A_{pq}(\theta, \varphi)s_{pq}(t - \frac{2r}{c} - \tau_{m'n'}) \tag{17}$$

where β_l is the reflection coefficient of the target during the lth transmit pulse period. Assume that β_l obeys

the Swerling-II target model. $\tau_{m'n'}$ is the propagation time delay between the reference point and the (m', n')-antenna. After separately matched filtering $x_{m'n'}(t)$ with the waveforms $\phi_{pq}(t)\exp\left(j2\pi f_{pq}t\right)$, the (p, q)-channel output of the (m', n')-antenna can be expressed as

$$x_{m'n'pql} = \beta_l \mathbf{w}_{pq}^H \mathbf{a}_{pq}(\theta, \varphi) b_{m'n'} A_{pq}(\theta, \varphi) R_{pq}(r) \quad (18)$$

where the constant term $\exp(-j4\pi f_c r/c)$ is absorbed into β_l for the sake of simplicity.

$$b_{m'n'} \approx \exp\left(j2\pi\left((m'-1)d_{21}(\theta, \varphi) + (n'-1)d_{12}(\theta, \varphi)\right)/\lambda_b\right)$$

is the (m', n')-element of the receive angular steering matrix $\mathbf{B}(\theta, \varphi)$, which has the form

$$\mathbf{B}(\theta, \varphi) = \mathbf{F}(2\pi f_b d_{21}(\theta, \varphi)/c, M) \circ \mathbf{F}(2\pi f_b d_{12}(\theta, \varphi)/c, N). \quad (19)$$

Similarly,

$$R_{pq}(r) = \exp\left(-j4\pi r\left((p-1)\Delta f_x + (q-1)\Delta f_z\right)/c\right)$$

is the (p, q)-element of the transmit steering matrix $\mathbf{R}(r)$ in range dimension, which can be written as

$$\mathbf{R}(r) = \mathbf{F}(-4\pi r \Delta f_x/c, P) \circ \mathbf{F}(-4\pi r \Delta f_z/c, Q). \quad (20)$$

Therefore, the overall transmit steering vector is

$$\begin{aligned}\mathbf{AR}(r, \theta, \varphi) &= \mathbf{R}(r) \odot \mathbf{A}(\theta, \varphi) \\ &= \mathbf{F}(-4\pi r \Delta f_x/c + 2\pi f_b K_x d_{21}(\theta, \varphi)/c, P) \\ &\quad \circ \mathbf{F}(-4\pi r \Delta f_z/c + 2\pi f_b K_z d_{12}(\theta, \varphi)/c, Q).\end{aligned} \quad (21)$$

It is obvious that the transmit steering vector is not only a function of the angle, but also a function of the range. When all subarrays are steered to the same angle (θ, φ), the conventional non-adaptive beamformer weight vector is

$$\mathbf{w}_{pq} = \mathbf{a}_{pq}(\theta, \varphi)/\left\|\mathbf{a}_{pq}(\theta, \varphi)\right\|_2. \quad (22)$$

Accordingly, (18) can be simplified as

$$x_{m'n'pql} = \beta_l b_{m'n'} A_{pq}(\theta, \varphi) R_{pq}(r). \quad (23)$$

Then (23) can be rewritten in a matrix form

$$\begin{aligned}\mathbf{X}_{m'n'l} = \beta_l b_{m'n'} \cdot \mathbf{F}(-4\pi r \Delta f_x/c + 2\pi f_b K_x d_{21}(\theta, \varphi)/c, P) \\ \circ \mathbf{F}(-4\pi r \Delta f_z/c + 2\pi f_b K_z d_{12}(\theta, \varphi)/c, Q).\end{aligned} \quad (24)$$

Furthermore, we can organize all output of the receive antennas in a tensor form

$$\boldsymbol{\mathcal{X}}_0 = \boldsymbol{\mathcal{A}}_0(\theta, \varphi, r) \circ \bar{\mathbf{s}}^T + \boldsymbol{\mathcal{N}}_0 \quad (25)$$

where $\boldsymbol{\mathcal{X}}_0 \in \mathbb{C}^{P\times Q\times M\times N\times L}$, $\bar{\mathbf{s}} = [\beta_l, \ldots, \beta_l] \in \mathbb{C}^{1\times L}$, L is the number of pulses, $\boldsymbol{\mathcal{N}}_0$ is a noise tensor with the same dimension as $\boldsymbol{\mathcal{X}}_0$, $\boldsymbol{\mathcal{A}}_0(\theta, \varphi, r) \in \mathbb{C}^{P\times Q\times M\times N}$ is the joint transmit-receive array steering tensor, constructed in the following fashion:

$$\boldsymbol{\mathcal{A}}_0(\theta, \varphi, r)\mathbf{G}_1(\mu_1) \circ \mathbf{G}_2(\mu_2) \circ \mathbf{G}_3(\mu_3) \circ \mathbf{G}_4(\mu_4) \quad (26)$$

where

$$\begin{aligned}\mathbf{G}_1(\mu_1) &= \mathbf{F}(-4\pi r \Delta f_x/c + 2\pi f_b K_x d_{21}(\theta, \varphi)/c, P) \\ \mathbf{G}_2(\mu_2) &= \mathbf{F}(-4\pi r \Delta f_z/c + 2\pi f_b K_z d_{12}(\theta, \varphi)/c, Q) \\ \mathbf{G}_3(\mu_3) &= \mathbf{F}(2\pi f_b d_{21}(\theta, \varphi)/c, M) \\ \mathbf{G}_4(\mu_4) &= \mathbf{F}(2\pi f_b d_{12}(\theta, \varphi)/c, N).\end{aligned}$$

Moreover, assume that there exists D targets located in far-field and the localization of the d-th target is denoted by $(\theta_d, \varphi_d, r_d)$ (25) can be extended to the multiple-target situation

$$\boldsymbol{\mathcal{X}} = \boldsymbol{\mathcal{A}} \times_5 \bar{\mathbf{S}}^T + \boldsymbol{\mathcal{N}} \quad (27)$$

where $\boldsymbol{\mathcal{X}} \in \mathbb{C}^{P\times Q\times M\times N\times L}$, $\bar{\mathbf{S}} = [\mathbf{c}_1, \mathbf{c}_2, \ldots, \mathbf{c}_L] \in \mathbb{C}^{D\times L}$, $\mathbf{c}_l = \left[\beta_{1,l}, \ldots, \beta_{D,l}\right]^T$, $\beta_{d,l}$ is the reflection coefficient to the d-th target during the lth pulse period. $\boldsymbol{\mathcal{A}} \in \mathbb{C}^{P\times Q\times M\times N\times D}$ is the array steering tensor, constructed in the following fashion:

$$\boldsymbol{\mathcal{A}} = [\boldsymbol{\mathcal{A}}_0(\theta_1, \varphi_1, r_1) \sqcup_5 \boldsymbol{\mathcal{A}}_0(\theta_2, \varphi_2, r_2) \ldots \sqcup_5 \boldsymbol{\mathcal{A}}_0(\theta_D, \varphi_D, r_D)] \quad (28)$$

where $\boldsymbol{\mathcal{A}} \sqcup_5 \boldsymbol{\mathcal{B}}$ is the concatenation of $\boldsymbol{\mathcal{A}}$ and $\boldsymbol{\mathcal{B}}$ along the 5-th mode. Consequently, the data model (27) can be expressed as the outer product operator

$$\boldsymbol{\mathcal{X}} = \sum_{d=1}^{D} \boldsymbol{\mathcal{A}}_0(\theta_d, \varphi_d, r_d) \circ \bar{\mathbf{s}}_d^T + \boldsymbol{\mathcal{N}} \quad (29)$$

where $\bar{\mathbf{s}}_d^T$ denotes the d-th row of $\bar{\mathbf{S}}$. In traditional matrix-based data models, all "spatial" dimensions 1, 2, 3, 4 are stacked along the rows and the snapshots (dimension 5) are aligned as the columns. Thus, the received data model can be written as the following matrix form

$$\mathbf{X} = \mathbf{A}\bar{\mathbf{S}} + \mathbf{N} \quad (30)$$

where $\bar{\mathbf{S}} = [\bar{\mathbf{s}}_1, \ldots \bar{\mathbf{s}}_d, \ldots, \bar{\mathbf{s}}_D]^T \in \mathbb{C}^{D\times L}$. The steering matrix $\mathbf{A}$ can be written as

$$\mathbf{A} = \mathbf{A}^{(1)} \oplus \mathbf{A}^{(2)} \oplus \mathbf{A}^{(3)} \oplus \mathbf{A}^{(4)} \quad (31)$$

where $\mathbf{A}^{(r)} = \left[\mathbf{G}_r\left(\mu_r^{(1)}\right), \mathbf{G}_r\left(\mu_r^{(2)}\right), \ldots, \mathbf{G}_r\left(\mu_r^{(D)}\right)\right]$, $r = 1, 2, 3, 4$, the vector $\mathbf{G}_r\left(\mu_r^{(d)}\right)$ represents the array response in the r-th dimension for the d-th target, where

$$\mu_1^{(d)} = -4\pi r_d \Delta f_x/c + 2\pi f_b K_x d_{21}(\theta_d, \varphi_d)/c \quad (32)$$

$$\mu_2^{(d)} = -4\pi r_d \Delta f_z/c + 2\pi f_b K_z d_{12}(\theta_d, \varphi_d)/c \quad (33)$$

$$\mu_3^{(d)} = 2\pi f_b d_{21}(\theta_d, \varphi_d)/c \quad (34)$$

$$\mu_4^{(d)} = 2\pi f_b d_{12}(\theta_d, \varphi_d)/c. \quad (35)$$

The target positions $\{(\theta_d, \varphi_d, r_d)\}_{d=1}^D$ can be located through an inverse transformation of the above identities

$$\hat{r}_{dx} = c\left(K_x \mu_3^{(d)} - \mu_1^{(d)}\right)/(4\pi\Delta f_x) \quad (36)$$

$$\hat{r}_{dz} = c\left(K_z \mu_4^{(d)} - \mu_2^{(d)}\right)/(4\pi\Delta f_z) \quad (37)$$

$$\hat{\theta}_d = \arcsin \frac{2\alpha_1 + \sqrt{4\alpha_1^2 - 4\left(1+\tan^2\beta\right)\left(\alpha_1^2+\alpha_2^2-\tan^2\beta\right)}}{2(1+\tan^2\beta)} \tag{38}$$

$$\hat{\varphi}_d = arc\cos\left(\mu_3^{(d)}/\pi\cos\hat{\theta}_d\right) \tag{39}$$

where $\alpha_1 = \mu_4^{(d)}/(\pi\cos\beta), \alpha_2 = \mu_3^{(d)}\tan\beta/\pi$, $\hat{r}_{dx}$ and $\hat{r}_{dz}$ are the range estimation values of the d-th target from the x' and z'-axes, respectively. Besides, the matrix data models can be represented as a transpose of the *5*-mode matrix unfolding of the tensor data models:

$$\begin{aligned}\mathbf{X} &= [\boldsymbol{\mathcal{X}}]_{(5)}^T \in \mathbb{C}^{PQMN\times L}\\ \mathbf{A} &= [\boldsymbol{\mathcal{A}}]_{(5)}^T \in \mathbb{C}^{PQMN\times D}\\ \mathbf{N} &= [\boldsymbol{\mathcal{N}}]_{(5)}^T \in \mathbb{C}^{PQMN\times L}\end{aligned} \tag{40}$$

where $[\boldsymbol{\mathcal{A}}]_{(n)}$ represents the matrix unfolding of the tensor $\boldsymbol{\mathcal{A}} \in \mathbb{C}^{I_1\times I_2\times\cdots\times I_N}$ along the nth mode which is consistent with [40]. For clarity, we further define $J_1 = P, J_2 = Q$, $J_3 = M, J_4 = N$, and $J = \prod_{r=1}^4 J_r$.

III. RANGE AMBIGUOUS ANALYSIS AND ELIMINATION

A. RANGE AMBIGUITY ANALYSIS

The range ambiguity problems due to FDA beampattern periodicity can be explained quantitatively. The phase differences between two adjacent channels in the same antenna along the *1*-mode and *2*-mode array response can be expressed in the following fashion because the phase observations are wrapped within $[-\pi, \pi)$ (see also (32) and (33)):

$$\mu_1^{(d)} = \mathrm{mod}\left(-4\pi r\Delta f_x/c + 2\pi f_b K_x d_{21}/c, 2\pi\right) \tag{41}$$

$$\mu_2^{(d)} = \mathrm{mod}\left(-4\pi r\Delta f_z/c + 2\pi f_b K_z d_{12}/c, 2\pi\right) \tag{42}$$

where $\mathrm{mod}(\cdot)$ denotes the complementary operation. Thus, the relationships between the true phase difference and frequency offsets are given by

$$\mu_1^{(d)} + 2k_x\pi = -4\pi r\Delta f_x/c + 2\pi f_b K_x d_{21}/c \tag{43}$$

$$\mu_2^{(d)} + 2k_z\pi = -4\pi r\Delta f_z/c + 2\pi f_b K_z d_{12}/c \tag{44}$$

where k_x and k_z are unknown integers. Therefore, if the uniform frequency offsets are employed, neither (43) nor (44) can unambiguously estimate the target range due to the phase wrapping, i.e., range ambiguity. In a general way, the angle estimation is unambiguous while the inter-element spacing is less than half a wavelength. In fact, this unambiguity is subject to the scope of $[-\pi/2, \pi/2]$, the angle estimation ambiguity will arise when the angle of the target exceeds the scope of $[-\pi/2, \pi/2]$. Likewise, it is enough to make sure that the maximum unambiguous range is larger than the maximum radar detection range. Assume that the maximum radar detection is $R_{\max}$, the integers k_x and k_z are in the scope of $\left[\frac{-2\Delta f_x R_{\max}}{c} - \frac{\Delta\varphi_x}{2\pi} + \frac{f_b K_x d_{21}}{c}, -\frac{\Delta\varphi_x}{2\pi} + \frac{f_b K_x d_{21}}{c}\right)$ and $\left[\frac{-2\Delta f_z R_{\max}}{c} - \frac{\Delta\varphi_z}{2\pi} + \frac{f_b K_z d_{12}}{c}, -\frac{\Delta\varphi_x}{2\pi} + \frac{f_b K_z d_{12}}{c}\right)$ due to $0 < r \le R_{\max}$. Since the range periodicity is $c/(2\Delta f)$, the frequency increment Δf needs to satisfy the boundary condition: $R_u = \frac{c}{2\Delta f} \ge R_{\max}$, i.e $\Delta f \le (c/2R_{\max})$. This implies that a larger frequency offset will result in a shorter maximum unambiguous range. However, a small frequency offset means poor range resolution. If $\Delta f_x = \Delta f_z = \Delta f = (c/2R_{\max})$, there are no range unambiguity. While for $\Delta f_x = \Delta f_z = N\Delta f$ with $N(>1)$ being an integer, there will be multiple ambiguous ranges. Let r_u denote one of the ambiguous ranges. According to (43), we have

$$\begin{cases}\mu_1^{(d)} + 2k_{x,d}\pi = -4\pi r_d\Delta f_x/c + 2\pi f_b K_x d_{21}/c\\ \mu_1^{(d)} + 2k_{x,u}\pi = -4\pi r_u\Delta f_x/c + 2\pi f_b K_x d_{21}/c.\end{cases} \tag{45}$$

Therefore, the relationship between the actual range and its ambiguous range can be modeled as

$$r_d - r_u = \frac{c}{2\Delta f}\cdot\frac{k_{x,u}-k_{x,d}}{N} = \frac{c}{2\Delta f}\cdot\frac{P_x}{N} \tag{46}$$

where P_x is an integer. According to the scope of k_x, P_x is subject to the range of $(-N, N)$, i.e., if $P_x \ne 0$, r_d is different from r_u, which means that the range estimation is not unique.

B. RANGE AMBIGUITY ELIMINATION WITH CO-PRIME FREQUENCY OFFSETS

The proposed planar FDS-MIMO radar offers an additional degree of freedom (DOF) along the z'-axe, which provides us a way to solve the conflict between range resolution and maximum unambiguous range in beam domain. To improve the range estimation precision and broaden unambiguity range, the idea of co-prime frequency offsets along the x' and z'-axes is proposed, i.e., $\Delta f_x = N_x\Delta f$ and $\Delta f_z = N_z\Delta f$, where N_x and N_z are co-prime integers. Different from [27], [34], where the co-prime frequency offsets are used for ULA, the merits of our method ensure that the characteristics of resolvability and uniform frequency offsets in each dimension are maintained, so that lots of existing algorithms can be used directly.

Theorem 1: Assume that r_d is the actual range of the dth source, multiple maxima at different ranges will present along the *1*-th mode and *2*-th mode array response including the actual range and multiple ambiguous ranges. However, by intersecting the two-mode array response, there uniquely exists one range $\hat{r}_d$ that presents a peak in both modes when the co-prime frequency offsets are employed. The proof is provided in Appendix A.

According to *Theorem 1*, we can locate D targets by uniquely finding D peaks in the MUSIC spectrum.

IV. PROPOSED TENSOR-BASED TARGET LOCALIZATION METHODS

A. PROPOSED UTMUSIC ALGORITHM

In existing subspace-based FDA target localization methods [24], [25], [38], they does not account for the multidimensional structure information inherent in the received data. Tensors have a rich history, while they have only recently become ubiquitous in signal and data analytics [41]. Obviously, tensor processing strategies is more appropriate in the FDS-MIMO radar due to the multidimensional data structure. Tensor decomposition mainly contains Tucker decomposition and Candecomp/Parafac (CP) decomposition.

However, parameter estimates based on CP model are usually obtained via iterative techniques that might need many iterations and do not guarantee convergence to the global optimum [42]. In this paper, we utilize the HOSVD to achieve tensor Tucker decomposition for target localization, which allows us to suppress the noise more efficiently than conventional SVD technique. The HOSVD of data tensor $\boldsymbol{\mathcal{X}} \in \mathbb{C}^{J\times L}$ is given by

$$\boldsymbol{\mathcal{X}} = \boldsymbol{\mathcal{S}} \times_1 \mathbf{U}_1 \times_2 \mathbf{U}_2 \times_3 \mathbf{U}_3 \times_4 \mathbf{U}_4 \times_5 \mathbf{U}_5 \tag{47}$$

where $\mathbf{U}_r \in \mathbb{C}^{J_r\times J_r}, r = 1,2,3,4$, $\mathbf{U}_5 \in \mathbb{C}^{L\times L}$ are the unitary matrices of n-mode singular vectors, and $\boldsymbol{\mathcal{S}}$ is the core tensor with the same sizes as $\boldsymbol{\mathcal{X}}$. $\mathbf{U}_i, i = 1,2,\ldots,5$ is the left singular vector of the i-mode matrix unfolding of $\boldsymbol{\mathcal{X}}$ which satisfies the all-orthogonality conditions [39]. The HOSVD-based low-rank approximation of $\boldsymbol{\mathcal{X}}$ can be expressed as

$$\boldsymbol{\mathcal{X}} \approx \boldsymbol{\mathcal{S}}^{[s]} \times_1 \mathbf{U}_1^{[s]} \times_2 \mathbf{U}_2^{[s]} \times_3 \mathbf{U}_3^{[s]} \times_4 \mathbf{U}_4^{[s]} \times_5 \mathbf{U}_5^{[s]} \tag{48}$$

where $\mathbf{U}_r^{[s]} \in \mathbb{C}^{J_r\times\rho_r}, \rho_r = \min\{J_r, D\}, r = 1,2,3,4$, $\mathbf{U}_5^{[s]} \in \mathbb{C}^{L\times D}$, and $\boldsymbol{\mathcal{S}}^{[s]} \in \mathbb{C}^{\rho_1\times\rho_2\times\rho_3\times\rho_4\times D}$. Then we define a tensor-based signal subspace

$$\boldsymbol{\mathcal{U}}^{[s]} \approx \boldsymbol{\mathcal{S}}^{[s]} \times_1 \mathbf{U}_1^{[s]} \times_2 \mathbf{U}_2^{[s]} \times_3 \mathbf{U}_3^{[s]} \times_4 \mathbf{U}_4^{[s]}. \tag{49}$$

In order to enhance the estimation accuracy, the forward-backward averaging can be used. Thus, the number of available snapshots is virtually doubled without sacrificing the array aperture. The forward-backward averaging of tensor $\boldsymbol{\mathcal{X}}$ is given by

$$\boldsymbol{\mathcal{Y}} = \left[\boldsymbol{\mathcal{X}} \sqcup_5 \left(\boldsymbol{\mathcal{X}}^* \times_1 \boldsymbol{\Pi}_{J_1} \times_2 \boldsymbol{\Pi}_{J_2} \times_3 \boldsymbol{\Pi}_{J_3} \times_4 \boldsymbol{\Pi}_{J_4} \times_5 \boldsymbol{\Pi}_L\right)\right]. \tag{50}$$

Note that the corresponding matrix-based data model is $\mathbf{Y} = \mathbf{Q}_J^H \left[\mathbf{X}\ \boldsymbol{\Pi}_J \mathbf{X}^* \boldsymbol{\Pi}_L\right] \mathbf{Q}_L^H \in \mathbb{C}^{J\times 2L}$. Since the forward -backward averaged tensor $\boldsymbol{\mathcal{Y}}$ is centro-Hermitian [40], the tensor $\boldsymbol{\mathcal{Y}}$ can be mapped onto the following real-valued tensor

$$\mathcal{T}\boldsymbol{\mathcal{Y}} = \boldsymbol{\mathcal{Y}} \times_1 \mathbf{Q}_{J_1}^H \times_2 \mathbf{Q}_{J_2}^H \times_3 \mathbf{Q}_{J_3}^H \times_4 \mathbf{Q}_{J_4}^H \times_5 \mathbf{Q}_{2L}^H. \tag{51}$$

The HOSVD of $\mathcal{T}\boldsymbol{\mathcal{Y}}$ is given by

$$\mathcal{T}\boldsymbol{\mathcal{Y}} = \boldsymbol{\mathcal{S}} \times_1 \mathbf{E}_1 \times_2 \mathbf{E}_2 \times_3 \mathbf{E}_3 \times_4 \mathbf{E}_4 \times_5 \mathbf{E}_5. \tag{52}$$

Similarly, the HOSVD-based low-rank approximation of $\mathcal{T}\boldsymbol{\mathcal{Y}}$ can be rewritten in the following fashion

$$\mathcal{T}\boldsymbol{\mathcal{Y}} \approx \boldsymbol{\mathcal{S}}_Y^{[s]} \times_1 \mathbf{E}_1^{[s]} \times_2 \mathbf{E}_2^{[s]} \times_3 \mathbf{E}_3^{[s]} \times_4 \mathbf{E}_4^{[s]} \times_5 \mathbf{E}_5^{[s]}. \tag{53}$$

Then, we define a real-valued tensor signal subspace

$$\boldsymbol{\mathcal{E}}^{[s]} \approx \mathbf{S}_Y^{[s]} \times_1 \mathbf{E}_1^{[s]} \times_2 \mathbf{E}_2^{[s]} \times_3 \mathbf{E}_3^{[s]} \times_4 \mathbf{E}_4^{[s]}. \tag{54}$$

Theorem 2: The relationship between the matrix-based real-valued signal subspace $\mathbf{E}_s$ of matrix $\mathbf{Y}$ and the tensor-based real-valued signal subspace $\left[\mathcal{E}^{[s]}\right]_5^T$ of tensor $\mathcal{T}\boldsymbol{\mathcal{Y}}$ are linked by the following equation

$$\left[\boldsymbol{\mathcal{E}}^{[s]}\right]_5^T = \left(\mathbf{E}_1^{[s]} \cdot \mathbf{E}_1^{[s]^H}\right) \otimes \ldots \otimes \left(\mathbf{E}_4^{[s]} \cdot \mathbf{E}_4^{[s]^H}\right) \cdot \mathbf{E}_s. \tag{55}$$

The proof is provided in Appendix B. One can observe that $\left[\boldsymbol{\mathcal{E}}^{[s]}\right]_5^T$ stems from the projection of $\mathbf{E}_s$ onto the Kronecker product of the space spanned by r-mode vectors $\mathbf{E}_r^{[s]}\mathbf{E}_r^{[s]^H}, r = 1,2,3,4$, which allows us to filter out noise in each mode of the measurement tensor $\boldsymbol{\mathcal{Y}}$ separately, so that enhanced noise suppression can be achieved for improved signal subspace estimation. Applying *Theorem 2*, the Unitary Tensor-MISIC (UTMUSIC) algorithm can be expressed in the following formulation, i.e.,

$$P_{MUSIC}(\theta,\varphi,r) = \frac{1}{\mathbf{d}(\theta,\varphi,r)^H \left(\mathbf{I}_J - \left[\boldsymbol{\mathcal{E}}^{[s]}\right]_{(5)}^T \cdot \left[\boldsymbol{\mathcal{E}}^{[s]}\right]_{(5)}^*\right) \mathbf{d}(\theta,\varphi,r)}. \tag{56}$$

Then the parameters with respect to (θ,φ,r) can be estimated from the peaks of (56)

$$(\hat{\theta}_d, \hat{\varphi}_d, \hat{r}_d) = \arg\max_{(\theta,\varphi,r)} |P_{MUSIC}(\theta,\varphi,r)| \tag{57}$$

where

$$\mathbf{d}(\theta,\varphi,r) = \left(\mathbf{Q}_{J_1}^H \otimes \mathbf{Q}_{J_2}^H \otimes \mathbf{Q}_{J_3}^H \otimes \mathbf{Q}_{J_4}^H\right) \cdot [\mathbf{G}_1(\mu_1) \otimes \mathbf{G}_2(\mu_2) \otimes \mathbf{G}_3(\mu_3) \otimes \mathbf{G}_4(\mu_4)]. \tag{58}$$

Through the HOSVD of $\mathcal{T}\boldsymbol{\mathcal{Y}}$, the structure inherent in the *5*D data is already utilized in the subspace estimation step to improve the localization performance.

B. DIMENSION-REDUCED METHODS FOR THE UTMUSIC

There is no doubt that the computation complexity of the proposed UTMUSIC algorithm in Section IV-A caused by the 3D spectral searching is prohibitively high. To alleviate this difficulty, we propose two computationally efficient methods.

1) Partial Spectral Search UTMUSIC Algorithm.

To tackle the high dimension subspace estimation, we can process the received data along the x' and z'-axe separately. Extracting the$q$-th *2*-mode slices (along the x'-axe) notating $\mathcal{T}\boldsymbol{\mathcal{Y}}^{(q)} \in \mathbb{C}^{J_1\times J_3\times J_4\times 2L}$ from the real-valued tensor $\mathcal{T}\boldsymbol{\mathcal{Y}}$, then we can obtain the corresponding real-valued tensor signal subspace $\left[\boldsymbol{\mathcal{U}}_x^{(q)}\right]_{(4)}^T$ in the similar way as Section IV-A. Therefore, the MUSIC spatial spectrum for the Q slices (along the x'-axe) is given by

$$P_{MUSIC,x}(\theta,\varphi) = \left|\sum_{q=1}^{Q} \frac{1}{\mathbf{d}_x(\theta,\varphi,r)^H \left(\mathbf{I}_{J_1J_3J_4} - \left[\boldsymbol{\mathcal{U}}^{(q)}\right]_{(4)}^T \cdot \left[\boldsymbol{\mathcal{U}}^{(q)}\right]_{(4)}^*\right) \mathbf{d}_x(\theta,\varphi,r)}\right| \tag{59}$$

where $\mathbf{d}_x(\theta,\varphi,r) = (\mathbf{Q}_{J_1}^H \otimes \mathbf{Q}_{J_3}^H \otimes \mathbf{Q}_{J_4}^H) \cdot (\mathbf{G}_1(\mu_1) \otimes \mathbf{G}_3(\mu_3) \otimes \mathbf{G}_4(\mu_4))$. Thus we have

$$(\hat{\theta}_d, \hat{\varphi}_d, \hat{r}_{dx}) = \arg\max_{(\theta,\varphi,r)} \left|P_{MUSIC,x}(\theta,\varphi,r)\right|. \tag{60}$$

Similarly, we can obtain

$$(\hat{\theta}_d, \hat{\varphi}_d, \hat{r}_{dz}) = \arg\max_{(\theta,\varphi,r)} \left|P_{MUSIC,z}(\theta,\varphi,r)\right|. \tag{61}$$

Searching for the peaks of all possible angles and ranges by (60) and (61) is feasible. However, the searching computational is still very high. Note that when the received data are processed in the above fashion, the frequency offsets in each axe are uniformed, thus the range periodicity can be exploited, i.e., the actual and ambiguous range peaks are uniformly distributed in the UTMUSIC range spectrum. Consequently, according to (43) and (44), we can recover all other possible ranges

$$\begin{cases} \hat{\mu}_d^{(1)} = \tilde{\mu}_d^{(1)} + 2k_x\pi \\ \hat{\mu}_d^{(2)} = \tilde{\mu}_d^{(2)} + 2k_z\pi \end{cases} \tag{62}$$

where $\tilde{\mu}_d^{(1)}$ and $\tilde{\mu}_d^{(2)}$ are obtained within $[-\pi, \pi)$. Note that the range differences between adjacent peaks are fixed as $c/(2\Delta f_x)$ or $c/(2\Delta f_z)$, there must exist one peak for each source at an arbitrary $c/(2\Delta f_x)$ or $c/(2\Delta f_z)$ area. Therefore, we can divide the total search scope into several small sectors of size $c/(2\Delta f_x) = R_{\max}/N_x$ and $c/(2\Delta f_z) = R_{\max}/N_z$ along x' and z'-axes respectively, and only search the first sector $R_{\max}/N_x$ and $R_{\max}/N_z$ to find the corresponding D peaks in x' and z'-axes respectively. Then, we can recover all other ambiguous peaks for each source by (62) without any other spectral search. Consequently, D targets can be uniquely located by finding the common D peaks by the partial spectral search UTMUSIC (PPS UTMUSIC), where it involves a limited spectral search over only a small sector.

2) Range-angle decoupling UTMUSIC Algorithm.

In the FDS-MIMO radar, the decoupled range-angle response can be mitigated due to the combination of FDA and MIMO radar. Consequently, the range and angle of targets can be solely estimated from the FDS-MIMO beamforming peaks. Moreover, the receive steering vector is independent of range as shown in (19). Therefore, the angle (θ_d, φ_d) and r_d can be estimated separately which we term the range-angle decoupling (RAD UTMUSIC) method, i.e., estimate angles (θ_d, φ_d) before the ranges r_d estimation. The (p, q)-channel received data $\boldsymbol{\mathcal{TY}}^{(p,q)} \in \mathbb{C}^{J_3\times J_4\times 2L}$ after the forward-backward averaging can be obtain by extracting the (p, q)-slices of real-valued tensor $\boldsymbol{\mathcal{TY}}$. The MUSIC spatial spectrum for the $P \times Q$ channels can be expressed as

$$P_{MUSIC,pq}(\theta, \varphi) = \left| \sum_{P=1}^{P} \sum_{q=1}^{Q} \frac{1}{\mathbf{d}(\theta,\varphi)^H \left(\mathbf{I}_{J_3J_4} - \left[\boldsymbol{\mathcal{U}}^{(p,q)}\right]_{(3)}^T \cdot \left[\boldsymbol{\mathcal{U}}^{(p,q)}\right]_{(3)}^* \right) \mathbf{d}(\theta,\varphi)} \right| \tag{63}$$

where $\left[\boldsymbol{\mathcal{U}}^{(p,q)}\right]_{(3)}^T$ is the (p, q)-real-valued tensor subspace of $\mathbf{TY}^{(p,q)}$, $\mathbf{d}(\theta, \varphi) = \left(\mathbf{Q}_{J_3}^H \otimes \mathbf{Q}_{J_4}^H\right) \cdot (\mathbf{G}_3(\mu_3) \otimes \mathbf{G}_4(\mu_4))$. We have

$$(\hat{\theta}_d, \hat{\varphi}_d) = \arg\max_{(\theta,\varphi)} |P_{MUSIC}(\theta, \varphi)|. \tag{64}$$

After obtaining the angle estimation $(\hat{\theta}_d, \hat{\varphi}_d)$, the received data with respect to $(\hat{\theta}_d, \hat{\varphi}_d)$ can be compensated, then the MUSIC cost function in range domain can be expressed as

$$P_{MUSIC}(r_d) \approx \left| \frac{1}{\mathbf{d}(r)^H \left(\mathbf{I}_{J_1J_2} - \left[\boldsymbol{\mathcal{U}}_r\right]_{(3)}^T \cdot \left[\boldsymbol{\mathcal{U}}_r\right]_{(3)}^* \right) \mathbf{d}(r)} \right| \tag{65}$$

where $\boldsymbol{\mathcal{U}}_r$ is the real-valued tensor-based signal subspace after the angle compensation, $\mathbf{d}(r) = \left(\mathbf{Q}_{J_1}^H \mathbf{F}(-4\pi r\Delta f_x/c, P)\right) \cdot \left(\mathbf{Q}_{J_2}^H \mathbf{F}(-4\pi r\Delta f_z/c, Q)\right)$.

C. COMPUTATIONAL COMPLEXITY ANALYSIS

In this subsection, we analyze the computational burden of the proposed PSS UTMUSIC and RAD UTMUSIC and compare them with the UTMUSIC, as well as the methods used in the FDA-based radar (MUSIC in [38] and MLE in [24]).

1) MUSIC IN [38]

for a uniform linear array with M antennas, the complexity of the SVD for an $M \times L$ data matrix is $O(MLD)$ [43]. All J' spectral search steps require the computational burden in the standard MUSIC algorithm is $J'(M+1)(M-D)$, where L denotes the number of snapshots, D is the number of sources, J' denotes the total sample points of spatial spectral over $[-\pi/2, \pi/2]$. In the FDS-MIMO radar, the data $\mathbf{X}$ is a $J \times L$ matrix. Therefore, the computational complexity in the MUSIC algorithm is given by $O\left(JLD + J_\theta J_\varphi J_r(J+1)(J-D)\right)$, where J_θ and J_φ denote the total sample points of spatial spectral over $[-\pi/2, \pi/2]$, and J_r denotes the total sample points of spatial spectral over $(0, R_{\max}]$.

2) MLE IN [24]

the target angles are estimated in receiver side and then the ranges are obtained in the joint transmit-receive dimensions. Firstly, the 5-dimension data $\boldsymbol{\mathcal{TY}}$ is decomposed into J_1J_23-dimension tensor $\boldsymbol{\mathcal{TY}}^{(p,q)}$ to estimate the angles. The matrix inverse operation of covariance matrix $\mathbf{R}_{pq}(\left[\boldsymbol{\mathcal{TY}}_{pq}\right]_3^T \left[\boldsymbol{\mathcal{TY}}_{pq}\right]_3^*/L)$ has the complexity of $O\left((J_3J_4)^3\right)$, the SVD of the whole channels output data need the computation complexity $O\left(J_1J_2\,(J_3J_4)^3\right)$, all the spectral search steps for the angles need $O\left(J_\theta J_\varphi JJ_3J_4\right)$. Similarly, for the ranges, the computational burden of the matrix inverse operation is $O\left((J_1J_2)^3\right)$, the search step needs $O\left(J_r\,(J_1J_2)^2\right)$. Thus the total computational complexity is $O\left(J_1J_2\,(J_3J_4)^3 + J_\theta J_\varphi JJ_3J_4 + (J_1J_2)^3 + J_r\,(J_1J_2)^2\right)$.

3) PSS UTMUSIC

in the x'-axe direction, the 5-dimension data $\boldsymbol{\mathcal{TY}}$ is decomposed into J_2 Q 4-dimension data $\boldsymbol{\mathcal{TY}}^{(q)}$. Computation cost of the HOSVD is $O(4JLD)$, which is same as the z'-axe direction. Thus the total computational burden is $O\left\{8JLD + J_\theta J_\varphi\left[(J+J_2)(J/J_2 - D) + (J+J_1)(J/J_1 - D)\right]\right\}$. when the PSS UTMIUSC method is used, the computational complexity is $O(8JLD + J_\theta J_\varphi J_r(J+J_2)(J/J_2 - D)/N_x + J_\theta J_\varphi J_r(J+J_1)\cdot(J/J_1 - D)/N_z)$.

4) RAD UTMUSIC

the 5-dimension data $\mathcal{TY}$ is decomposed into J_1J_2 3-dimension tensor $\mathcal{TY}^{(p,q)}$. The HOSVD of $\mathcal{TY}_{pq}$ has the complexity of $O(3JLD/J_1J_2)$, the SVD of the whole channels output data need the computation complexity $O(3JLD)$, all the spectral search steps for the angles have the computational burden of the standard MUSIC algorithm is $O\left(J_\theta J_\varphi (J + J_1J_2)(J_3J_4 - D)\right)$. For the ranges, the computational burden of the SVD is $O(3JLD/J_3J_4)$, the search steps need $O(J_r(J_1J_2+1)(J_1J_2-D))$. Thus the total computational cost is $O\{3JLD + J_\theta J_\varphi (J + J_1J_2)(J_3J_4 - D) + 3JLD/J_3J_4 + J_r(J_1J_2+1)\cdot(J_1J_2-D)\}$.

The computation complexity mainly lies in the parameter search, which is much heavier than that of the SVD or the HOSVD due to $\min\{J_\theta, J_\varphi, J_r\} \gg J$. Their computational complexities are approximately computed in Table 1.

TABLE 1. Computational complexity comparison.

Methods	Complexity
MLE in [24]	$O\left(\left(J_\theta J_\varphi J J_3 J_4 + J_r (J_1J_2)^2\right)\right)$
MUSIC in [38]	$O\left(J_\theta J_\varphi J_r J (J-D)\right)$
UTMUSIC	$O\left(J_\theta J_\varphi J_r J (J-D)/4\right)$
PSS UTMUSIC	$O\left(J_\theta J_\varphi J_r J \left((J/J_2 - D)/N_x + (J/J_1 - D)/N_z\right)/4\right)$
RAD TMUSIC	$O\left(\left(J_\theta J_\varphi J (J_3J_4 - D)/(J_1J_2) + J_r J_1 J_2 (J_1J_2 - D)\right)/4\right)$

V. NUMERICAL SIMULATIONS

In this section, several simulations are conducted. Unless stated otherwise, we use the following simulation parameters: $f_c = 300$ MHz, $\Delta f = 3$ kHz, the maximum unambiguous range $R_u = 50$ km, $\beta = 10°$. The antennas at each axes are spaced half a wavelength. The noise is modeled as zero-mean spatially white complex Gaussian process. $D = 3$ uncorrelated targets are supposed which are located at $\{\theta_d\}_{d=1}^3 = \{10°, 30°, 60°\}$, $\{\varphi_d\}_{d=1}^3 = \{45°, 60°, 80°\}$, $\{r_d\}_{d=1}^3 = \{20.0, 20.5, 21.2\}$ km, respectively.

A. JOINT TRANSMIT-RECEIVE 4-D BEAMPATTERN

To better grasp the advantage of FDS-MIMO radar over traditional PAR and MIMO radar in terms of beampattern, the 4-D pattern visualization technique is employed to show the joint transmit-receive beampattern of FDS-MIMO radar and conventional MIMO radar. The proposed FDS-MIMO radar consists of $J_3 \times J_4 = 12 \times 12$ antennas, which is divided into $J_1 \times J_2 = 6 \times 6$ uniform rectangular subarrays. One target of interest is supposed to reflect the transmit signals and impinge on the radar from location $(\theta_1, \varphi_1, r_1)$. Fig. 2 shows the joint transmit-receive 4D beampattern cut at -25dB in the FDS-MIMO radar and traditional MIMO radar, respectively. It is seen that from Fig. 2 that: 1) The target angle can be obtained from the beamforming peak in the traditional MIMO radar, while the range cannot be directly estimated due to the range- independent beampattern. 2) The beampattern of FDS-MIMO radar has range-angle dependence and the mainbeam is quasi-ellipsoid in 4D view which can be used to locate the target directly from the beamforming peak. 3) The range and angle coupling is mitigated owing to the jointly utilization of FDA and MIMO. The detail with enlarged scale in Fig. 2 (a) shows the -3dB beamwidth cut at φ_1, one can observe that range resolution is about $R_u/(P+Q-1) = 4.55$km which does not satisfy the requirement of target localization. In order to improve range resolution, more antennas and larger frequency increments should be employed. Fig. 3 (a) depicts the pattern under uniform increment $(N_x, N_z) = (4, 4)$, the range resolution is enhanced while the range ambiguity problem arises. However, when the strategy of co-prime frequency offsets $(N_x, N_z) = (4, 3)$ is used, the range ambiguity is eliminated and range resolution is approximately $R_u/((P-1)N_x + (Q-1)N_z) \approx 1.43$km as shown in Fig. 3(b). Accordingly, the contradiction between the range resolution and maximum unambiguous range can be resolved by our method.

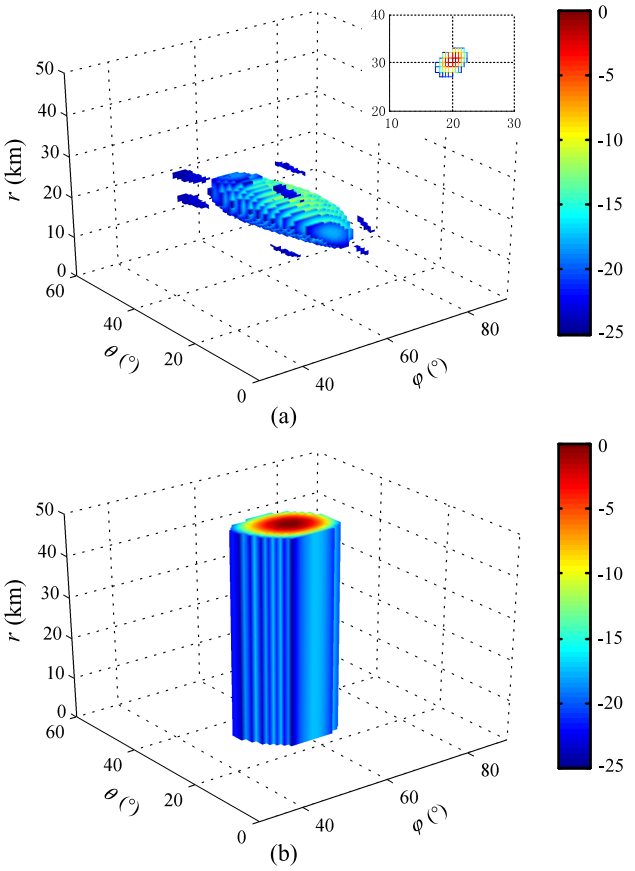

FIGURE 2. Beampattern comparison cut at -25dB in 4D view. (a) FDS-MIMO radar. (b) Traditional MIMO radar.

B. PERFORMANCE ANALYSIS OF TENSOR SUBSPACE ESTIMATION

In this simulation, we examine the accuracy of the estimated signal subspace obtained by different methods,

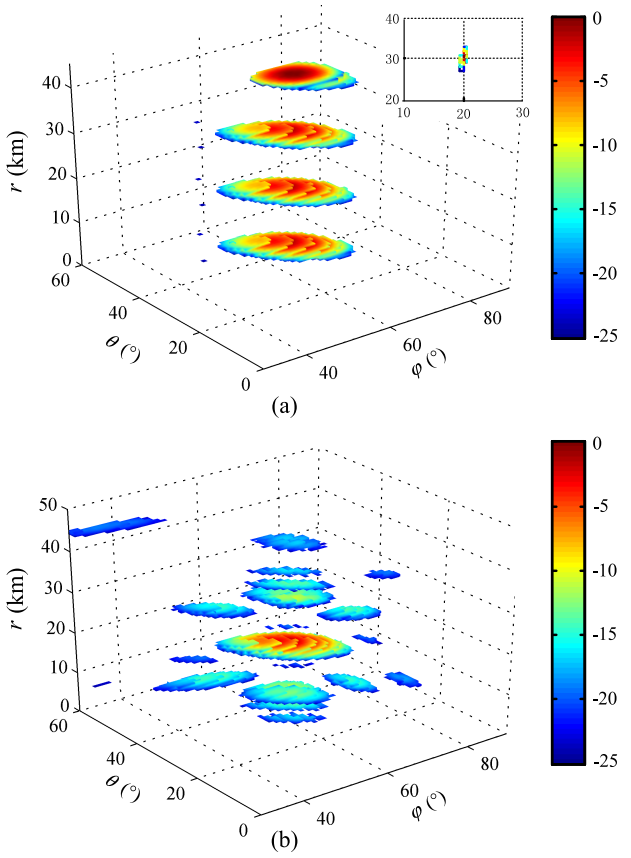

FIGURE 3. Beampattern cut at -25dB in 4D view. (a) $(N_x, N_z) = (4, 4)$. (b) $(N_x, N_z) = (4, 3)$.

e.g., the proposed HOSVD-based low-rank approximation method and the traditional SVD-based method, via the corresponding root mean square error (RMSE) which is defined as

$$\|\Delta \mathbf{E}_s\|_F = \left\|\tilde{\mathbf{E}}_s - \mathbf{E}_s\right\|_F$$

where $\Delta \mathbf{u}_d = \tilde{\mathbf{u}}_d \frac{\tilde{\mathbf{u}}_d^H \mathbf{u}_d}{|\tilde{\mathbf{u}}_d^H \mathbf{u}_d|} - \mathbf{u}_d$ is the d-th column of real-valued signal subspace error matrix $\Delta \mathbf{E}_s$, $\mathbf{u}_d$ denotes the d-th column of the true real-valued signal subspace $\mathbf{E}_s$, $\tilde{\mathbf{u}}_d$ denotes the d-th column of the estimated real-valued signal subspace $\tilde{\mathbf{E}}_s$ obtained by (76) and $\left[\boldsymbol{\mathcal{E}}^{[s]}\right]_5^T$ obtained by (77), respectively. We employ the parameters $J_1 = J_2 = 4, J_3 = J_4 = 8$ with the number of pulses $L = 10$, and $(N_x, N_z) = (7, 5)$. Fig. 4. plots the RMSE of signal subspace estimation versus SNR when the number of pulses is $L = 10$. One can observe that the accuracy of the HOSVD-based low-rank approximation is clearly advantageous over the matrix-based SVD. This advantage is due to the fact that the multidimensional structure information of the received data is exploited and the matrix unfoldings of the received data tensor is processed 'jointly'. Our received multidimensional signal obeys this unique characteristic while the noise does not—this can be utilized to filter out more of the noise. This is something the matrix-based SVD of the stacked matrix representation does not exploit.

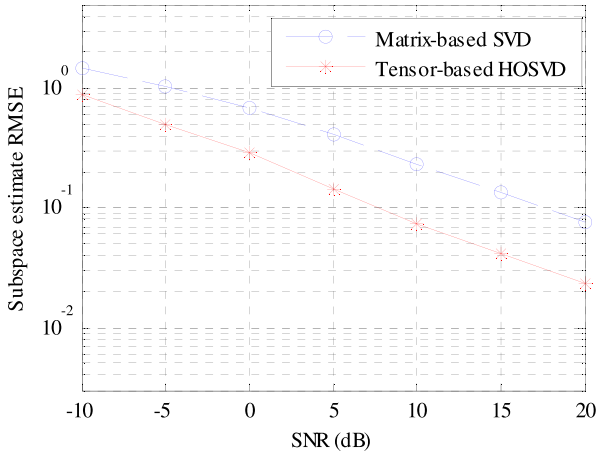

FIGURE 4. RMSE of the signal subspace estimation versus SNR.

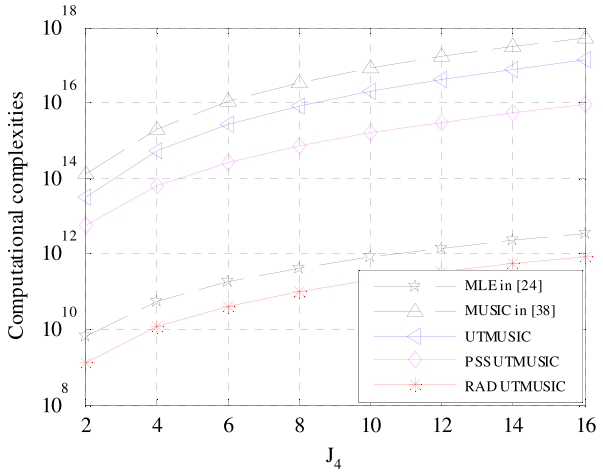

FIGURE 5. Computational complexities versus J_4.

C. PERFORMANCE ANALYSIS OF UTMUSIC-BASED ALGORITHMS

This simulation is carried out to compare the computing complexities and target localization performance among the proposed methods (UTMUSIC, PSS UTMUSIC, RAD UTMUSIC) and the methods used in the FDA-based radar (MUSIC in [38] and MLE in [24]). The used performance criterion is also the RMSE, which is calculated by the following equations

$$\text{RMSE}(\theta, \varphi) = \sqrt{\frac{1}{2DM_c}\sum_{i=1}^{M_c}\sum_{d=1}^{D}\left[\left(\hat{\theta}_{i,d} - \theta_d\right)^2 + \left(\hat{\varphi}_{i,d} - \varphi_d\right)^2\right]}$$

$$\text{RMSE}(r) = \sqrt{\frac{1}{DM_c}\sum_{i=1}^{M_c}\sum_{d=1}^{D}\left(\hat{r}_{i,d} - r_d\right)^2}$$

where $\hat{\theta}_{i,d}$, $\hat{\varphi}_{i,d}$, and $\hat{r}_{i,d}$ represent the estimations of the elevation angle, azimuth angle, and range for the d-th target in the i-th Monte Carlo trial, respectively, $M_c = 200$ Monte Carlo trials are conducted in the following simulations.

Suppose $J_3 = 8$, $J_1 = 4$, and $J_2 = J_4/2$, i.e., each subarray consists of 2×2 antennas. According to the computational complexities shown in Table 1. Fig. 5 plots the complexities of the above methods versus J_4 for spectral search interval 0.05° and 10m, respectively. It is obvious that the complexity of the RAD UTMUSIC algorithm is lower than that of other approaches, followed by the MLE in [24], PSS UTMUSIC, UTMMUSIC, and MUSIC in [38].

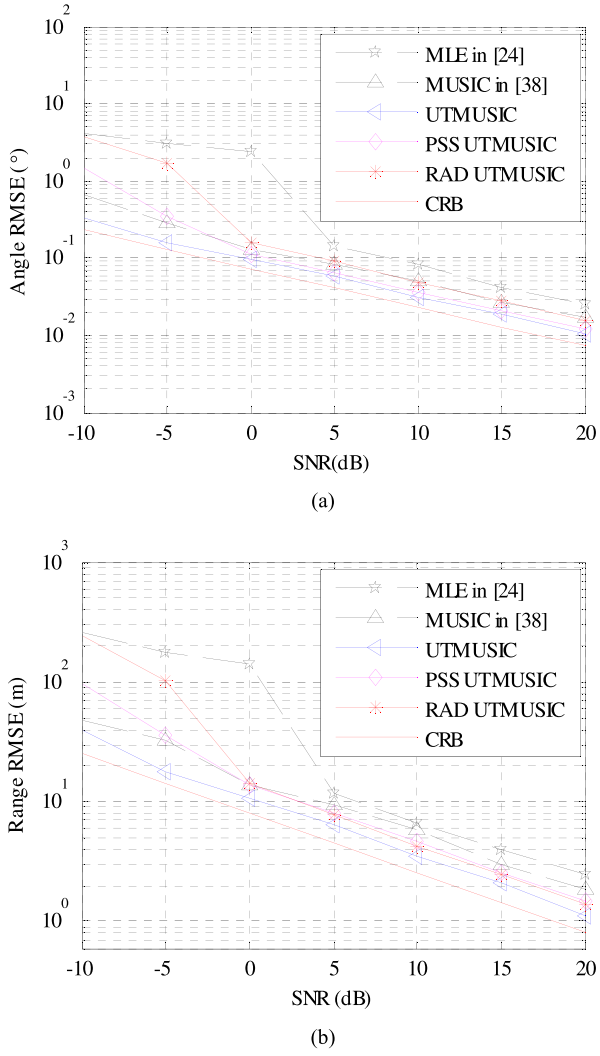

FIGURE 6. RMSE of parameters estimation versus SNR. (a) Angle dimension. (b) Range dimension.

Finally, we investigate the PSS and RAD based methods. We use the same parameter as Section V-B, hence the complexities of the MLE, MUSIC, UTMUSIC, PSS UTMUSIC, and RAD UTMUSIC are approximately $O\left(4.25 \times 10^{11}\right)$, $O\left(3.39 \times 10^{16}\right)$, $O\left(8.47 \times 10^{15}\right)$, $O\left(7.19 \times 10^{14}\right)$, $O\left(1.01 \times 10^{11}\right)$, respectively. Fig. 6 depicts the RMSE of the five methods versus SNR. It can be seen that: 1) The localization performance of the proposed UTMUSIC is better than that of other approaches and afford about 5dB improvement compared with the matrix-based MUSIC in [38]. 2) The proposed PSS UTMUSIC is superior to the RAD UTMUSIC in low SNR region, while the RAD UTMUSIC has the lowest complexity. Besides, the PSS and RAD UTMUSIC exhibit better performance when the SNR is higher than 0dB but with a significantly lower complexity as compared to the MUSIC algorithm in [38]. 3) As a dimension-reduced method, the RAD UTMUSIC outperforms the MLE in [24] at lower computational complexities. The improvement of our methods comes from the improved subspace estimation in the HOSVD-based low-rank approximation method and the forward-backward averaging technique. Thus, in high SNR, the RAD UTMUSIC algorithm is the best choice with satisfactory accuracy and significantly lower computational burden. In low SNR, we can choose the UTMUSIC method to obtain higher localization performance. Besides, the proposed PSS UTMUSIC method makes a good tradeoff between computation complexity and estimation accuracy.

VI. CONCLUSIONS

In this paper, we investigated the target localization in 3D using a planner FDS-MIMO radar system. The FDA range ambiguity problem, originated from range periodicity of the beampattern, is analyzed, and a co-prime frequency increment design strategy is proposed to circumvent the above problem. Using tensor-based representation and HOSVD-based low-rank approximation subspace estimation, an extension to traditional MUSIC algorithm, called unitary tensor MUSIC (UTMUSIC), is proposed. Moreover, two modifications of this algorithm are made to reduce the computational complexity. The proposed methods successfully exploit FDS-MIMO inherent multidimensional structure to achieve outperformed performance over the SVD-based MUSIC and MLE in terms of accuracy and complexity. Note that the Doppler information is ignored in this paper, which may be further investigation in our future work.

APPENDIX A

In this Appendix, we show that the targets can be located uniquely when co-prime frequency offsets are employed along the x' and z'-axes.

A. EXISTENCE

Since r_d is the range of the dth target echo impinging on the receive planar array, it will present a peak in the MUSIC spectrum of the range due to the spatial spectrum estimation without dependence on array configuration. Therefore, the peak in the MUSIC spectrum at the position of r_d will present along *1*-th mode and *2*-th array response. Thus there exists at least one common peak at the same position of the spatial spectrum for the two modes.

B. UNIQUENESS

Suppose that there exists two distinct common peaks $\hat{r}_{d,1}$ and $\hat{r}_{d,2}$. According to (46), the relationship between

$\hat{r}_{d,1}$ and $\hat{r}_{d,2}$ for x'-axes can be expressed as

$$\hat{r}_{d,1} - \hat{r}_{d,2} = \frac{c}{2\Delta f} \cdot \frac{P_x}{N_x}. \tag{66}$$

Similarly, for the frequency increments $\Delta f_z = N_z \Delta f$ with $N_z (> 1)$ being an integer, we can obtain

$$\hat{r}_{d,1} - \hat{r}_{d,2} = \frac{c}{2\Delta f} \cdot \frac{P_z}{N_z} \tag{67}$$

where P_z is subject to the ranges of $(-N_z, N_z)$. Therefore we have

$$\frac{P_x}{N_x} = \frac{P_z}{N_z}. \tag{68}$$

Note that N_x and N_z are denoted as mutually co-prime integers. Besides, P_x and P_z are subject to $(-N_x, N_x)$ and $(-N_z, N_z)$, respectively. According to the co-prime property between N_x and N_z, (68) has no solution except for $P_x = P_z = 0$, which means that

$$r_d = \hat{r}_{d,1} = \hat{r}_{d,2}. \tag{69}$$

Therefore, there uniquely exists one common range r_d for both the two modes, which is he desired result. Hence, the proof of the *Theorem 1* is completed.

APPENDIX B

In this Appendix, we discuss the relationships between the two signal subspaces. According to (52), the HOSVD-based low-rank approximation of $\boldsymbol{\mathcal{S}}_Y^{[s]}$ can be computed as

$$\boldsymbol{\mathcal{S}}_Y^{[s]} \approx \boldsymbol{\mathcal{TY}} \times_1 \mathbf{E}_1^{[s]^H} \times_2 \mathbf{E}_2^{[s]^H} \times_3 \mathbf{E}_3^{[s]^H} \times_4 \mathbf{E}_4^{[s]^H} \times_5 \mathbf{E}_5^{[s]^H}. \tag{70}$$

Inserting (70) into (54) yields

$$\boldsymbol{\mathcal{E}}^{[s]} = \boldsymbol{\mathcal{TY}} \times_1 \left(\mathbf{E}_1^{[s]} \cdot \mathbf{E}_1^{[s]^H}\right) \ldots \times_4 \left(\mathbf{E}_4^{[s]} \cdot \mathbf{E}_4^{[s]^H}\right) \times_5 \left(\sum\nolimits_5^{[s]^{-1}} \cdot \mathbf{E}_5^{[s]^H}\right) \tag{71}$$

Here we add the inverse of the matrix $\sum_5^{[s]}$, which is the diagonal matrix including the D dominant singular values of the 5-mode matrix unfolding of $\boldsymbol{\mathcal{Y}}$. Note that this scaling has no impact on the real-valued tensor signal subspace. After 5-mode unfolding of $\boldsymbol{\mathcal{U}}^{[s]}$ and using the following property of the n-mode product

$$\begin{aligned}&[\boldsymbol{\mathcal{A}} \times_1 \mathbf{X}_1 \times_2 \mathbf{X}_2 \times \ldots \times_R \mathbf{X}_R]_{(n)} \\ &= \mathbf{X}_n \cdot [\boldsymbol{\mathcal{A}}]_{(n)} \cdot (\mathbf{X}_{n+1} \otimes \mathbf{X}_{n+2} \cdots \otimes \mathbf{X}_R \otimes \mathbf{X}_1 \cdots \otimes \mathbf{X}_{n-1}).\end{aligned} \tag{72}$$

Then we obtain

$$\left[\boldsymbol{\mathcal{E}}^{[s]}\right]_5^T = \left(\left(\mathbf{E}_1^{[s]} \cdot \mathbf{E}_1^{[s]^H}\right) \otimes \ldots \otimes \left(\mathbf{E}_4^{[s]} \cdot \mathbf{E}_4^{[s]^H}\right)\right) \cdot [\boldsymbol{\mathcal{TY}}]_{(5)}^T \cdot \mathbf{E}_5^{[s]^*} \cdot \sum\nolimits_5^{[s]^{-1}}. \tag{73}$$

The SVD of $\mathbf{Y}$ is given

$$\mathbf{Y} = [\boldsymbol{\mathcal{TY}}]_{(5)}^T \approx \mathbf{E}_s \cdot \sum\nolimits_s \cdot \mathbf{F}_s^H \tag{74}$$

where $\mathbf{U}_s \in \mathbb{C}^{J \times D}$, $\sum_s \in \mathbb{C}^{D \times D}$, and $\mathbf{V}_s \in \mathbb{C}^{L \times D}$. Note that $[\boldsymbol{\mathcal{TY}}]_{(5)} = \mathbf{E}_5^{[s]} \sum_5^{[s]} \mathbf{F}_5^{[s]^H}$, we have

$$\mathbf{E}_5^{[s]^*} = \mathbf{F}_s. \tag{75}$$

Consequently, we have

$$\left[\boldsymbol{\mathcal{E}}^{[s]}\right]_5^T = \left(\left(\mathbf{E}_1^{[s]} \cdot \mathbf{E}_1^{[s]^H}\right) \otimes \ldots \otimes \left(\mathbf{E}_4^{[s]} \cdot \mathbf{E}_4^{[s]^H}\right)\right) \cdot \mathbf{E}_s. \tag{76}$$

which is the desired result. This completes the proof of *Theorem 2*.

REFERENCES

[1] H. Krim and M. Viberg, "Two decades of array signal processing research: The parametric approach," *IEEE Signal Process. Mag.*, vol. 13, no. 4, pp. 67–94, Jul. 1996.

[2] Y. Zhu, L. Liu, A. Wang, K. Sayana, and J. C. Zhang, "DoA estimation and capacity analysis for 2D active massive MIMO systems," in *Proc. IEEE Int. Conf. Commun.*, Jun. 2013, pp. 4630–4634.

[3] P. Antonik, M. C. Wicks, H. D. Griffiths, and C. J. Baker, "Frequency diverse array radars," in *Proc. IEEE Radar Conf.*, Verona, NY, USA, Apr. 2006, pp. 215–217.

[4] P. Antonik, M. C. Wicks, H. D. Griffiths, and C. J. Baker, "Multi-mission multi-mode waveform diversity," in *Proc. IEEE Radar Conf.*, Verona, NY, USA, Apr. 2006, pp. 580–582.

[5] M. Secmen, S. Demir, A. Hizal, and T. Eker, "Frequency diverse array antenna with periodic time modulated pattern in range and angle," in *Proc. IEEE Radar Conf.*, Boston, MA, USA, Apr. 2007, pp. 427–430.

[6] P. Antonik and W. C. Wicks, "Method and apparatus for simultaneous synthetic aperture radar and moving target indication," U.S. Patent 2008 0 129 584, Jun. 5, 2008.

[7] T. Eker, S. Demir, and A. Hizal, "Exploitation of linear frequency modulated continuous waveform (LFMCW) for frequency diverse arrays," *IEEE Trans. Antennas Propag.*, vol. 61, no. 7, pp. 3546–3553, Jul. 2013.

[8] W.-Q. Wang, "Frequency diverse array antenna: New opportunities," *IEEE Antennas Propag. Mag.*, vol. 57, no. 2, pp. 145–152, Apr. 2015.

[9] P. Antonik, "An investigation of a frequency diverse array," Ph.D. dissertation, Dept. Electron. Elect. Eng., Univ. College London, London, U.K., 2009.

[10] W. Q. Wang, "Overview of frequency diverse array in radar and navigation applications," *IET Radar, Sonar Navigat.*, vol. 10, no. 6, pp. 1001–1012, 2016.

[11] W.-Q. Wang, "Range-angle dependent transmit beampattern synthesis for linear frequency diverse arrays," *IEEE Trans. Antennas Propag.*, vol. 61, no. 8, pp. 4073–4081, Aug. 2013.

[12] Y. H. Xu, X. Shi, J. Xu, and P. Li, "Range-angle-dependent beamforming of pulsed frequency diverse array," *IEEE Trans. Antennas Propag.*, vol. 63, no. 7, pp. 3262–3267, Jul. 2015.

[13] A.-M. Yao, W. Wu, and D.-G. Fang, "Frequency diverse array antenna using time-modulated optimized frequency offset to obtain time-invariant spatial fine focusing beampattern," *IEEE Trans. Antennas Propag.*, vol. 64, no. 10, pp. 4434–4446, Oct. 2016.

[14] W. Khan, I. M. Qureshi, and S. Saeed, "Frequency diverse array radar with logarithmically increasing frequency offset," *IEEE Antennas Wireless Propag. Lett.*, vol. 14, pp. 499–502, 2015.

[15] W. Khan and I. M. Qureshi, "Frequency diverse array radar with time-dependent frequency offset," *IEEE Antennas Wireless Propag. Lett.*, vol. 13, pp. 758–761, 2014.

[16] H. Shao, J. Dai, J. Xiong, H. Chen, and W.-Q. Wang, "Dot-shaped range-angle beampattern synthesis for frequency diverse array," *IEEE Antennas Wireless Propag. Lett.*, vol. 15, pp. 1703–1706, Feb. 2016.

[17] K. D. Gao, W.-Q. Wang, H. Chen, and J. Cai, "Transmit beamspace design for multi-carrier frequency diverse array sensor," *IEEE Sensors J.*, vol. 16, no. 14, pp. 5709–5714, Jul. 2016.

[18] J. Farooq, M. A. Temple, and M. A. Saville, "Application of frequency diverse arrays to synthetic aperture radar imaging," in *Proc. Int. Electromagn. Adv. Appl. Conf.*, Turin, Italy, Sep. 2007, pp. 447–449.
[19] J. Farooq, M. A. Temple, and M. A. Saville, "Exploiting frequency diverse array processing to improve SAR image resolution," in *Proc. IEEE Radar Conf.*, Rome, Italy, May 2008, pp. 1–5.
[20] J. W. Xu, G. Liao, S. Zhu, and H. C. So, "Deceptive jamming suppression with frequency diverse MIMO radar," *Signal Process.*, vol. 113, pp. 9–17, Aug. 2015.
[21] W. Q. Wang, "Phased-MIMO radar with frequency diversity for range-dependent beamforming," *IEEE Sensors J.*, vol. 13, no. 4, pp. 1320–1328, Apr. 2013.
[22] C. Cetintepe and S. Demir, "Multipath characteristics of frequency diverse arrays over a ground plane," *IEEE Trans. Antennas Propag.*, vol. 62, no. 7, pp. 3567–3574, Jul. 2014.
[23] P. F. Sammartino, C. J. Baker, and H. D. Griffiths, "Frequency diverse MIMO techniques for radar," *IEEE Trans. Aerosp. Electron. Syst.*, vol. 49, no. 1, pp. 201–222, Jan. 2013.
[24] J. Xu, G. Liao, S. Zhu, L. Huang, and H. C. So, "Joint range and angle estimation using MIMO radar with frequency diverse array," *IEEE Trans. Signal Process.*, vol. 63, no. 13, pp. 3396–3410, Jul. 2015.
[25] W.-Q. Wang and H. C. So, "Transmit subaperturing for range and angle estimation in frequency diverse array radar," *IEEE Trans. Signal Process.*, vol. 62, no. 8, pp. 2000–2011, Apr. 2014.
[26] W.-Q. Wang and H. Z. Shao, "Range-angle localization of targets by a double-pulse frequency diverse array radar," *IEEE J. Sel. Topics Signal Process.*, vol. 8, no. 1, pp. 106–114, Feb. 2014.
[27] S. Qin, Y. D. Zhang, and M. G. Amin, "Multi-target localization using frequency diverse coprime arrays with coprime frequency offsets," in *Proc. IEEE Radar Conf.*, Philadelphia, PA, USA, May 2016, pp. 1–5.
[28] W.-Q. Wang, H. C. So, and H. Shao, "Nonuniform frequency diverse array for range-angle imaging of targets," *IEEE Sensors J.*, vol. 14, no. 8, pp. 2469–2476, Aug. 2014.
[29] K. Gao, W.-Q. Wang, J. Cai, and J. Xiong, "Decoupled frequency diverse array rangeŰangle-dependent beampattern synthesis using non-linearly increasing frequency offsets," *IET Microw., Antennas Propag.*, vol. 10, no. 8, pp. 880–884, Mar. 2016.
[30] Y. Wang, G. Huang, and W. Li, "Transmit beampattern design in range and angle domains for MIMO frequency diverse array radar," *IEEE Antennas Wireless Propag. Lett.*, vol. 16, pp. 1003–1006, 2016, doi: 10.1109/LAWP.2016.2616193.
[31] J. Xiong, W.-Q. Wang, H. Shao, and H. Chen, "Frequency diverse array transmit beampattern optimization with genetic algorithm," *IEEE Antennas Wireless Propag. Lett.*, vol. 16, pp. 469–472, Jun. 2016, doi: 10.1109/LAWP.2016.2584078.
[32] W. Khan, I. M. Qureshi, A. Basit, and M. Zubair, "A double pulse MIMO frequency diverse array radar for improved range-angle localization of target," *Wireless Pers. Commun.*, vol. 82, no. 4, pp. 4073–4081, Aug. 2013.
[33] W. Q. Wang, "Subarray-based frequency diverse array radar for target range-angle estimation," *IEEE Trans. Aerosp. Electron. Syst.*, vol. 50, no. 4, pp. 3057–3067, Oct. 2014.
[34] S. Qin, Y. D. Zhang, M. G. Amin, and F. Gini, "Frequency diverse coprime arrays with coprime frequency offsets for multitarget localization," *IEEE J. Sel. Topics Signal Process.*, vol. 11, no. 2, pp. 321–335, Mar. 2017, doi: 10.1109/JSTSP.2016.2627184.
[35] W.-Q. Wang and C. Zhu, "Nested array receiver with time-delayers for joint target range and angle estimation," *IET Radar, Sonar Navigat.*, vol. 10, no. 8, pp. 1384–1393, 2016, doi: 10.1049/iet-rsn.2015.0450.
[36] L. Huang, X. Li, P.-C. Gong, and Z. He, "Frequency diverse array radar for target range-angle estimation," *Int. J. Comput. Math. Elect. Electron. Eng.*, vol. 35, no. 3, pp. 1257–1270, Feb. 2016.
[37] A. M. Jones and B. D. Rigling, "Planar frequency diverse array receiver architecture," in *Proc. IEEE Radar Conf.*, Atlanta, GA, USA, May 2012, pp. 145–150.
[38] X. Li, D. Wang, and X. Ma, "Three-dimensional target localization and Cramér-Rao bound for two-dimensional OFDM-MIMO radar," *Int. J. Antennas Propag.*, vol. 2017, Mar. 2017, Art. no. 4171452, doi: 10.1155/2017/4171452.
[39] L. De Lathauwer, B. De Moor, and J. Vandewalle, "A multilinear singular value decomposition," *SIAM J. Matrix Anal. Appl.*, vol. 21, no. 4, pp. 1253–1278, 2000.
[40] M. Haardt and, F. Roemer, and G. Del Galdo, "Higher-order SVD-based subspace estimation to improve the parameter estimation accuracy in multidimensional harmonic retrieval problems," *IEEE Trans. Signal Process.*, vol. 56, no. 7, pp. 3198–3213, Jul. 2008.
[41] N. D. Sidiropoulos, L. De Lathauwer, X. Fu, K. Huang, E. E. Papalexakis, and C. Faloutsos, "Tensor decomposition for signal processing and machine learning," *IEEE Trans. Signal Process.*, vol. 65, no. 13, pp. 3551–3582, Jal. 2017.
[42] M. Rajih, "Blind identification of underdetermined mixtures based on the characteristic function," Ph.D. dissertation, Univ. Nice Sophia Antipolis, Nice, France, Dec. 2006.
[43] G. H. Golub and C. F. Van Loan, *Matrix Computations*. Baltimore, MD, USA: The Johns Hopkins Univ. Press, 1996.

XINGXING LI received the B.S. degree from the Air Force Radar Academy, Wuhan, China, in 2011, the M.S. degrees from the Air Force Early Warning Academy, Wuhan, in 2013, where he is currently pursuing the Ph.D. degree.

His research interests include MIMO radar signal processing, adaptive beamforming, target localization, and target feature extraction and identification.

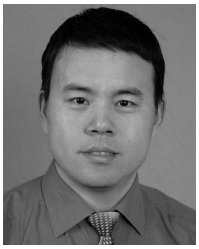

DANGWEI WANG received the B.S. and M.S. degrees from Wuhan Radar Academy, Wuhan, China, in 2000 and 2003, respectively, and the Ph.D. degree from Department of Electrical and Electronic Engineering, National University of Defense Technology, Changsha, China, in 2006. He is currently an Associate Professor with the Air Force Early Warning Academy, Wuhan, China.

His research interests include multi-channels radar target characteristic and advanced signal processing with application to radar target imaging and identification.

WEN-QIN WANG (M'08–SM'16) received the B.S. degree in electrical engineering from Shandong University, Jinan, China, in 2002, and the M.E. and Ph.D. degrees in information and communication engineering from the University of Electronic Science and Technology of China (UESTC), Chengdu, China, in 2005 and 2010, respectively.

He was with the National Key Laboratory of Microwave Imaging Technology, Chinese Academy of Sciences, Beijing, China, from 2005 to 2007. Since 2007, he has been with the School of Communication and Information Engineering, UESTC, where he is currently a Full Professor. From 2011 to 2012, he was a Visiting Scholar with the Stevens Institute of Technology, NJ, USA. From 2012 to 2013, he was a Hong Kong Scholar with the City University of Hong Kong, Hong Kong. From 2014 to 2016, he was a Marie Curie Fellow with the Imperial College London, U.K. He has authored two books published, respectively, by Springer and CRC Press. His current research interests span the area of array signal processing and circuit system for radar, communications and microwave remote sensing.

Dr. Wang was a recipient of the National Young Top-Notch Talent of the Ten-Thousand Talent Program Award. He is on the editorial board of four international journals.

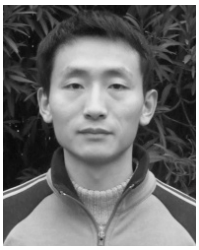

WEIJIAN LIU (M'14) received the B.S. degree in information engineering and the M.S. degree in signal and information processing from Wuhan Radar Academy, Wuhan, China, in 2006 and 2009, respectively, and the Ph.D. degree in information and communication engineering from the National University of Defense Technology, Changsha, in 2014.

He is currently a Lecturer with the Wuhan Electronic Institute. His current research interests include multichannel signal detection, statistical, and array signal processing.

XIAOYAN MA received the B.S. degree from the Nanjing University of Science and Technology, Nanjing, China, in 1982, the M.S. degree from the National University of Defense Technology, Changsha, China, in 1988, and the Ph.D. degree from Tsinghua University, Beijing, China in 2002. He is currently a Full Professor and the Dean of the Air Force Early Warning Academy, Wuhan, China.

His main research interests include radar system design, target detection, and imaging, and ISAR signal processing.